Michael El-Sheik, MD
Johannes T. Heverhagen, MSc
Heiko Alfke, MD
Jens J. Froelich, MD, PhD
Joachim Hornegger, PhD
Thomas Brunner, PhD
Klaus Jochen Klose, MD, PhD
Hans-Joachim Wagner, MD, PhD

Index terms:
Computed tomography (CT), helical
Computed tomography (CT), technology
Computed tomography (CT) thin-section

Published online before print
10.1148/radiol.2213010606
Radiology 2001; 221:843–849

Abbreviations:
CRO = computed rotational osteography
3D = three-dimensional

[1] From the Department of Diagnostic Radiology, Philipps-University Marburg, Germany (M.E., J.T.H., H.A., J.J.F., K.J.K., H.J.W.); Siemens Medical Solutions, Forchheim, Germany (J.H., T.B.); and Department of Radiology, University of Wisconsin Hospital and Clinics, E3/311 Clinical Science Center, 600 Highland Ave, Madison, WI 53792-3252 (H.J.W.). Received March 14, 2001; revision requested April 9; revision received June 13; accepted June 22. **Address correspondence to** H.J.W. (e-mail: *hwagner@mail.radiology.wisc.edu*).

© RSNA, 2001

Author contributions:
Guarantors of integrity of entire study, M.E., H.J.W.; study concepts, M.E., H.J.W.; study design, M.E., J.T.H., H.A., K.J.K.; literature research, M.E., J.T.H., T.B.; clinical studies, M.E., H.A., J.J.F.; experimental studies, M.E.; data acquisition, M.E., H.J.W., H.A.; data analysis/interpretation, M.E., J.J.F., H.A., T.B., J.H., K.J.K.; manuscript preparation, M.E., J.H., T.B., J.J.F., H.A.; manuscript definition of intellectual content, M.E., J.T.H., H.J.W.; manuscript editing, M.E., H.J.W.; manuscript revision/review and final version approval, all authors.

Multiplanar Reconstructions and Three-dimensional Imaging (Computed Rotational Osteography) of Complex Fractures by Using a C-arm System: Initial Results[1]

With use of a calibrated angiographic C-arm system and a postprocessing workstation, the authors acquired volume data sets from two-dimensional digital projection images obtained during a C-arm rotation around the patient axis. Multiplanar reconstruction and three-dimensional images of complex fractures were reconstructed and compared with spiral computed tomographic studies in a cadaveric pig study and in eight patients. Computed rotational osteography provided high-resolution multiplanar reconstruction and three-dimensional images of complex fractures.

Detailed assessment of complex fractures requires acquisition of multiple views to depict the anatomic relationship of fracture fragments and to obtain a three-dimensional (3D) assessment of the fracture. Cross-sectional imaging modalities, such as computed tomography (CT) and magnetic resonance imaging, provide superior evaluation of fracture morphology in the preoperative setting (1–3). With current developments in multi–detector row CT technology, previous limitations in spatial resolution along the patient's longitudinal axis, which led to anisotropic voxels with related secondary reconstruction artifacts, have been eliminated.

Intraoperative monitoring of interventional or orthopedic fixation procedures is usually performed with projection imaging modalities, such as C-arm fluoroscopy or biplane radiography. Owing to insufficient imaging guidance in some cases, however, misplacement of orthopedic fixation devices or misalignment of fracture fragments may occur, which necessitates secondary revisions.

In recent years, computed rotational angiography has been developed. This technique allows computation of 3D images from projection radiographs (4–6). This method was originally developed for vascular imaging (7,8). Owing to high contrast between bones and surrounding soft tissue, however, the technique for computed rotational angiography might be applicable to osteopathology.

The purpose of this study was to evaluate the initial results with 3D multiplanar reconstruction images of complex fractures acquired with a C-arm system. We called this method computed rotational osteography (CRO).

Materials and Methods

Imaging System

With CRO, it is possible to acquire a 3D volume data set of bones from two-dimensional projection radiographs. The process was divided into three steps.

First, multiview two-dimensional projection radiographs were acquired with a commercially available angiographic system (Multistar; Siemens Medical Solutions, Forchheim, Germany) with the option of 3D angiography. Second, these projection radiographs were transferred to a dedicated postprocessing workstation (3DVirtuoso; Siemens Medical Solutions) where a volume data set was reconstructed, which resulted in a CT-type data set consisting of many sections. Third, the volume data set was visualized by using the volume-rendering technique and multiplanar reconstruction images.

TABLE 1
Programs in the C-arm System to Perform Rotational Projection Radiography

Organ Program Rotational Time*	No. of Projection Radiographs	Rotation Angle	Rotation Angle for Each Projection Radiograph	CT Dose Index (mGy)†
7 seconds				
Low dose	64	160°	2.5°	2.0
High dose	64	160°	2.5°	5.2
9 seconds				
Low dose	90	180°	2.0°	2.9
High dose	90	180°	2.0°	7.3
12 seconds				
Low dose	120	180°	1.5°	3.9
High dose	120	180°	1.5°	9.7

* Low dose = 0.48-μGy nominal dose per CRO image. High dose = 1.2 μGy nominal dose per CRO image. In all programs, tube voltage was 70 kV, and the field of view of the x-ray image intensifier was 40 cm.

† Absorbed dose for a cylindric phantom with a 16-cm diameter on the axis, for a 40-cm nominal zoom; for a 28-cm zoom, ×2; for a 20-cm zoom, ×4.

Projection Radiograph Acquisition

As many as 120 digital projection radiographs were acquired during each forward and backward rotation (to 180°) of the ceiling-mounted C-arm system around the longitudinal axis of an object (z axis). For digital subtraction imaging, the forward rotation is used to generate mask images, while instant backward rotation provided contrast-enhanced data sets. Different imaging protocols were available with different rotation times, numbers of images acquired during each rotation, and doses (Table 1). Furthermore, the zoom setting of the 40-cm image intensifier could be varied between 20, 28, and 40 cm. The matrix of the projection radiographs was 1,024 × 1,024 pixels, and the pixel size depended on the zoom factor.

The distance between the focal spot and the detector was about 123 cm and that between the focal spot and isocenter was about 80 cm. The magnification factor was approximately ×1.5. The digital projection radiographs were stored on the angiographic system computer (POLYTRON TOP, version 3.0; Siemens Medical Solutions).

The C-arm system with its specific properties was specially calibrated for 3D acquisitions. Calibration was performed on site during installation of the 3D option and must be repeated approximately annually. Calibration must be performed for several properties of the imaging system. Distortion correction adjusts the pincushion distortion of the image intensifier and television detector and the influence of the magnetic field of the earth on the electron optics. Distortion correction depends on the position and orientation of the C-arm in space and on the zoom format. The sensitivity of the detector changes over the field of view; therefore, a gain correction is calibrated. Moreover, the projection geometry (ie, the mapping from two-dimensional to 3D) of the whole imaging system must be characterized to ensure that the position of heavy masses in motion is measured with a high degree of accuracy and that the acquisition geometry is sufficiently well reproduced in consecutive acquisitions. Faulty calibration of the acquisition system may cause severe artifacts on reconstruction images.

Volume Data Set Reconstruction

When 3D acquisitions were transferred from the angiographic system to the 3D workstation, correction steps were performed on the two-dimensional projection radiographs: distortion correction, gain correction, and transformation into CT line integrals (9,10). The 3D data set was reconstructed on the basis of these modified projection data, which resulted in a CT-type data set consisting of as many as 512 transverse sections. The reconstruction algorithm was a modified Feldkamp cone-beam CT convolution backprojection (11). The projection geometry was taken into account in the backprojection process.

The technical performance of the reconstruction system was not the focus of this study. Studies that were performed with a prototype system that is similar to the present system offer more details (11,12). These studies included measurements of spatial resolution and contrast-to-noise ratio.

The maximum field of view that can be reconstructed depends on the distance between the focal spot and detector and between the focal spot and isocenter, the magnification factor, and the image intensifier zoom. Use of a 40-cm nominal zoom results in acquisition of a rough sphere around the isocenter, with a diameter of approximately 26 cm. Depending on the object, image truncation cannot always be avoided (ie, parts of the object may not be visualized on all projection images). As long as high-contrast objects are reconstructed, the corresponding artifacts are tolerable.

The volume of interest that should be reconstructed can be selected on two orthogonal projection radiographs, which are shown on the screen of the workstation. The size of the volume of interest is limited by the field of view of the projection radiographs. A further limitation is that, for technical reasons, the resulting CT-type volume data set is limited to a maximum of 512 transverse sections. With isotropic voxels, the length of the volume of interest in the patient's longitudinal axis (z axis) will be maximal 512 times the voxel side length (eg, for a voxel side length of 0.3 mm and the 256 × 256 matrix, the cuboid has a maximal dimension of 7.7 × 7.7 × 15.4 cm).

The size of the volume of interest in combination with the size of the section matrix (128 × 128, 256 × 256, or 512 × 512) determines the voxel size. The minimal length of a voxel is about 110 μm. The two-dimensional detector has isotropic pixels; therefore, the reconstructed voxels are also isotropic. The isotropic voxel size could not prevent the spatial resolution from decreasing farther outside the central plane, owing to data limitations of cone-beam CT.

The reconstruction time depended on the number of two-dimensional projection radiographs acquired, the size of the object that should be demonstrated (volume of interest), the reconstruction matrix, and the reconstruction kernel (high speed or high quality). Reconstruction times varied between 3 minutes (64 projection radiographs, 128 × 128 matrix, and high-speed kernel) and longer than 30 minutes (120 projection radiographs,

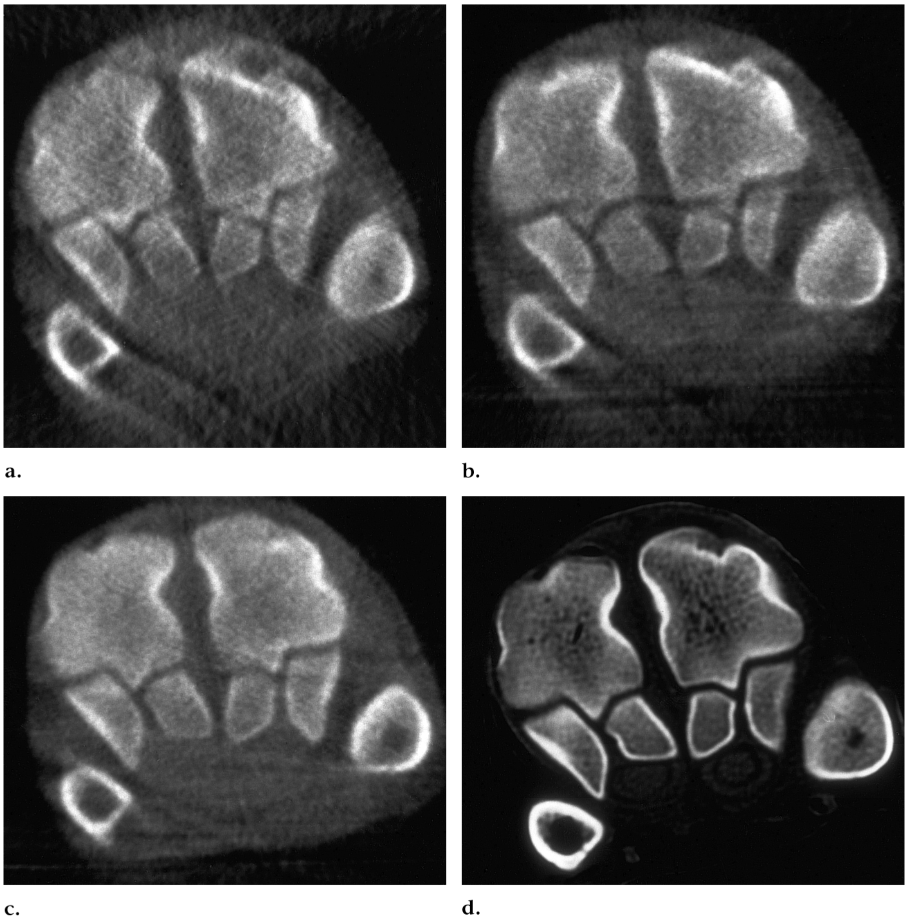

Figure 1. Effect of different imaging protocols on image quality and artifacts on CRO images obtained in a pig foot. **(a–c)** Transverse reconstruction images were acquired with the high-dose program at **(a)** 7 seconds, at **(b)** 9 seconds, and at **(c)** 12 seconds. The 512 × 512 matrix and the high-quality kernel were used in all cases. **(d)** Corresponding thin-section CT image. Acquisition of more projection images or rotations improves the quality of the multiplanar reconstruction images and reduces the artifacts. Nevertheless, on **a–c** compared with **d**, the margins of the bones are depicted less sharply, and contrast resolution is reduced.

512 × 512-voxel matrix, and high-quality kernel) for a 15 × 15 × 15-cm cuboid. Meanwhile, the workstation has been upgraded, and typical reconstruction times are less than 3 minutes.

Visualization of the Volume Data Set

Finally, visualization of the volume data set was performed by creating 3D images (volume-rendering technique) or two-dimensional multiplanar reconstruction images in different orientations, as is known from CT.

Animal Study

We evaluated different rotational imaging protocols available with the C-arm system and the software of the angiographic system. An overview of the acquisition modes is given in Table 1. In addition, we investigated the different reconstruction options with the workstation. The evaluation of rotational imaging programs and reconstruction options was aimed at optimizing imaging and reconstruction parameters for visualization of osseous structures.

We performed a postmortem animal study by using the feet of recently slaughtered young pigs obtained from the slaughterhouse. Six feet from six different pigs underwent CRO and thin-section spiral CT before and after fractures were induced by means of direct force with a hammer. The different imaging parameters for CRO are illustrated in Table 1. Additionally, for the 3D 12-second program, tube voltage was varied between 50, 70, and 90 kV. Reconstruction of the transverse CRO images on the postprocessing workstation was varied by using different matrices (128 × 128, 256 × 256, and 512 × 512) and two different kernels (high speed and high quality). The volume of interest was adapted to the size of the pig feet (approximately 15 × 7 × 7 cm) and was identical for all reconstruction images except those with the 512 × 512 matrix. The volume of interest had to be reduced for the highest matrix (7 × 7 × 7 cm) in the z axis because the volume data set was limited to 512 transverse sections. In these cases, we visualized only the central part of the feet.

CT was performed with a single-array spiral CT scanner (Somatom Plus; Siemens Medical Solutions). Scanning parameters included collimation, 1 mm; table feed, 2 mm; increment, 1 mm; circulation time, 0.75 second; tube voltage, 140 kV; and tube current, 159 mA. Transverse CT images were obtained with the scanner software and were sent to the postprocessing workstation to acquire multiplanar reconstruction and 3D images.

Transverse images obtained with both imaging modalities (CRO and CT) were used to generate multiplanar reconstruction and 3D images on the workstation. Multiplanar reconstruction images were created in sagittal and coronal orientations, with a section thickness of 2 mm. The 3D images were created by means of volume-rendering algorithms (two-dimensional texture mapping). The observers could change display parameters (center and width, opacity, brightness) when they reviewed the images at the workstation. Reconstruction time and computation time for creation of the 3D and multiplanar reconstruction images were measured for both modalities and the various protocols.

Two radiologists (M.E., J.J.F.) independently evaluated the CRO images without knowledge of imaging and reconstruction parameters. The observers arranged corresponding transverse and multiplanar reconstruction images on the basis of the different 3D programs regarding spatial and contrast resolution. Criteria for spatial resolution were visualization of the physis and small bones and visualization of the fracture lines and small fragments. Criteria for contrast resolution were differentiation of cortical and spongiosal bone, visualization of the outlines of the bones, and discrimination of various soft tissues (eg, fascia, fat, and musculature). Furthermore, the observers arranged the images regarding the occurrence of beam-hardening artifacts and steps in the surface of the bone on volume-rendered images.

Figure 2. Comparison of CRO and CT on the basis of multiplanar reconstruction and 3D images obtained in a patient. **(a, b)** CRO-derived images (coronal reconstruction image [**a**] and volume-rendered image with an opacity grade of 90% [**b**]) were obtained with the high-dose program at 12 seconds with a 256 × 256 matrix and the high-quality kernel. **(c, d)** Corresponding reconstruction images derived from thin-section spiral CT scans. Owing to isotropic voxels and the high spatial resolution, **a** and **b** show details such as the physis (arrow in **a** and **c**) better than do **c** and **d**. Despite the artifacts on the transverse images (Fig 1), the multiplanar reconstruction and 3D images are of high quality. Compared with CT scans, details of the fracture, such as nondisplaced fractures, might be overlooked on CRO-derived reconstruction images because the margins of the bones (arrow in **b** and **d**) are less distinct.

In a second step, CRO images that were judged to have the best spatial and contrast resolution and fewer artifacts were compared directly with the corresponding spiral CT images regarding spatial and contrast resolution. The CRO images were rated as not as good as, equal to, or better than the spiral CT reconstruction images. On the basis of results in our animal study, scanning parameters that resulted in images with the best spatial and contrast resolution and fewer artifacts were selected for human applications.

Human Studies

To evaluate CRO for the imaging of complex fractures in vivo, six consecutive patients (two men, four women; mean age, 57.6 years; age range, 43–78 years) with fractures of the spine (n = 3) or tibial plateau (n = 3) and two additional patients (one 42-year-old woman and one 50-year-old man) after surgical treatment of spinal fractures (bisegmental posterior internal fixation of vertebral fractures of the thoracolumbar junction) underwent CRO (with parameters based on the results in our animal study) and thin-section CT. Inclusion criteria were complex fractures of the tibial plateau or spine that required cross-sectional imaging. Exclusion criteria were pregnancy and age younger than 18 years. The institutional review board approved the study. Written informed consent was obtained from all patients. The imaging and reconstruction parameters for CRO were the following: 3D high-dose program at 12 seconds; rotation time, 12 seconds; number of projection images, 120; rotation angle, 180°; rotation angle per image, 1.5°; tube voltage, 70 kV; tube current, 108 mA; image intensifier, 40 cm; reconstruction kernel, high quality; reconstruction matrix, 256 × 256. The re-

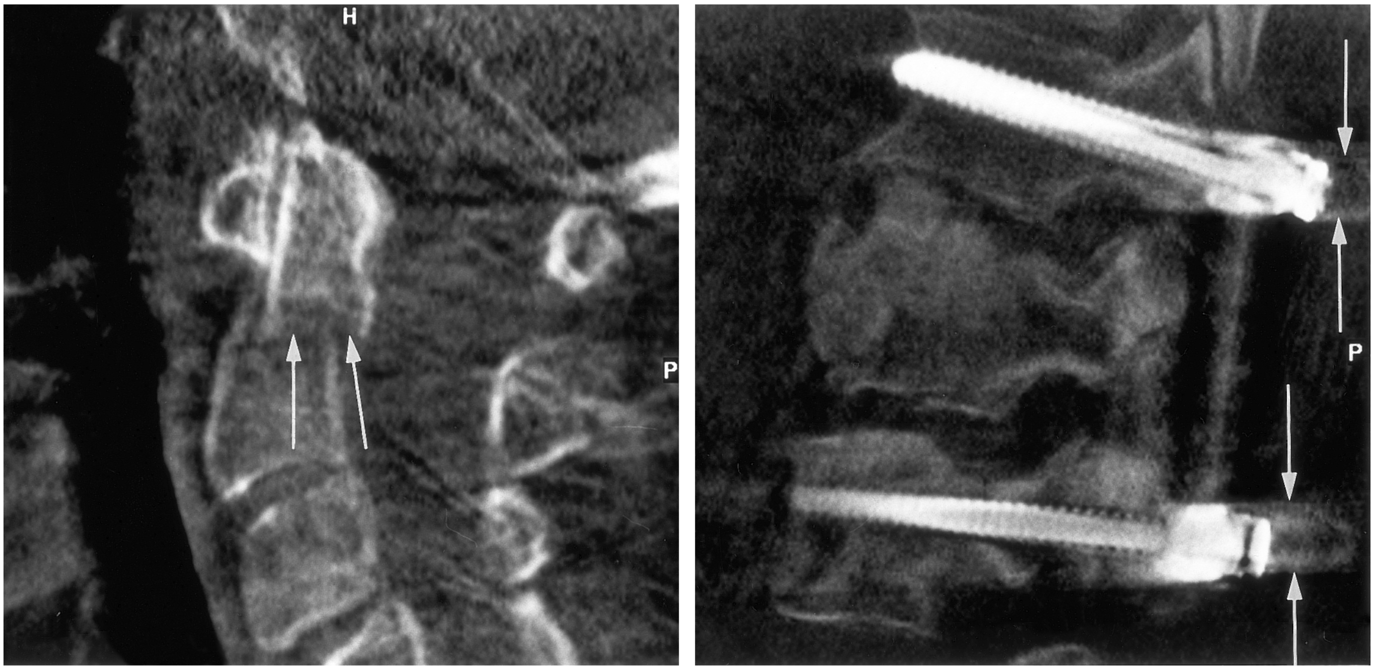

a. b.

Figure 3. CRO-derived images of complex fractures in a patient. **(a)** CRO-derived image (high-dose program at 12 seconds, 256 × 256 matrix, high-quality kernel) of the cervical spine clearly demonstrates the odontoid fracture (arrows) with slight subluxation of the odontoid process. **(b)** CRO-derived image (high-dose program at 12 seconds, 256 × 256 matrix, high-quality kernel) of the thoracolumbar spine was obtained after bisegmental posterior stabilization for a burst fracture of T12. The positions of the pedicle screws are shown, with only minor artifacts (arrows) due to the metal implants.

TABLE 2
Fracture Classification on the Basis of CT or CRO Images

Patient No.	Fracture Location	Classification with CRO Images	Classification with CT Images
1	Tibial plateau	Type B, group 3	Type B, group 3
2	Tibial plateau	Type B, group 2	Type B, group 2
3	Spine, C2	Type 2 (Anderson)	Type 2 (Anderson)
4	Spine, T2	Type A, group 1, subgroup 3	Type A, group 1, subgroup 3
5	Spine, L1	Type B, group 2, subgroup 1	Type B, group 2, subgroup 1
6	Tibial plateau	Type C, group 2	Type C, group 2

construction matrix in human studies was 256 × 256 because, for technical reasons, the volume of interest was limited for the 512 × 512-voxel matrix.

Spiral CT parameters included the following: collimation, 2 mm; table feed, 3 mm; increment, 1 mm; circulation time 0.75 second; tube voltage, 140 kV; and tube current, 159–240 mA. Transverse images were reconstructed with use of the scanner software and were transferred to the postprocessing workstation to generate multiplanar reconstruction and 3D images.

Multiplanar reconstruction images were created in sagittal and coronal orientations with a section thickness of 2 mm. The 3D images were created with use of volume-rendering algorithms. Two radiologists (M.E., J.J.F.) independently evaluated both methods separately. Both CT and CRO images were analyzed for the location of the fractures and bones involved. Spinal and tibial fractures were classified according to the classification system of the Association for the Study of Internal Fixation (Davos, Switzerland) (13,14) or the classification proposed by Anderson and D'Alonzo for fractures of C2 (15). When disagreement occurred, a consensus reading was obtained. Both reviewers compared images obtained with the two modalities and decided whether CRO reconstruction images were not as good as, equal to, or better than the CT reconstruction images with regard to spatial resolution (ie, visualization of the fracture lines and detection of small osseous fragments) and contrast resolution (ie, visualization of the outlines of the bones, differentiation of cortical and spongiosal bone, and differentiation of various soft tissues).

In the two postoperative cases, the observers judged if the alignment of the fracture and the position of the internal fixation devices could be assessed. They also compared results with both modalities with regard to artifacts that were caused by the osteosynthetic devices.

Results

Animal Studies

According to both observers, the best spatial and contrast resolution were achieved with the 3D high-dose program at 12 seconds, which has the longest rotation time (12 seconds for 180°) to obtain the most projection images ($n = 120$, or one image every 1.5°). In addition, results were optimized if the high-dose modes were selected and the tube current was 70 kV.

Reduced rotation angle, reduced number of projection images acquired per rotation, and reduced amperage were associated with reduced differentiation between cortical and spongiosal structures of the bones and increased artifact. Furthermore, the outlines of the bones became less distinct, and details such as the physis or fracture lines could not be differentiated as well (Fig 1). Both protocols allowed discrimination between bone and soft tissue, but neither protocol allowed differentiation among various soft tissues. The image quality seemed to be influenced more by the number of projection images and less by the tube voltage and amperage.

Regarding image reconstruction at the workstation, optimized spatial resolution was obtained with the 512×512 matrix and the high-quality kernel. Nevertheless, reconstruction of the whole foot of the pig was not possible with the 512×512 matrix, owing to technical limitations.

Compared with CT images, transverse CRO images depicted the outlines of bones less distinctly and showed more beam-hardening artifacts at areas of compact bone (Fig 1). Despite these artifacts, CRO sagittal and coronal reconstruction images, in comparison with CT images, were associated with fewer artifacts and provided higher spatial resolution with clearer visualization of details (eg, the physis) (Fig 2). On the other hand, in comparison with CT 3D images, nondisplaced fractures might be missed on CRO 3D images because bone fragments were depicted less sharply (Fig 2). Contrast resolution was superior with CT. Differentiation of various types of soft tissue was possible on only CT images.

The time required for reconstruction of transverse CRO images was dependent on the 3D program, reconstruction matrix, size of the volume of interest, and reconstruction kernel. Reconstruction time varied between 130 seconds (low-dose program at 7 seconds, 128×128 matrix, high-speed kernel) and about 600 seconds (high-dose program at 12 seconds, 256×256 matrix, high-quality kernel) for identical volume of interest ($7 \times 7 \times 15$ cm). The computation time for generation of multiplanar reconstruction and 3D images was affected by the number of transverse images acquired but did not depend on the modality (CRO or CT).

Human Studies

There was no difference between the modalities in fracture classification on the images obtained in the six preoperative patients. A detailed evaluation of fracture classification is provided in Table 2. There were no discrepancies between the two observers.

In the two postoperative cases, both CRO and CT images helped determine the exact position of the orthopedic fixation devices. The alignment of the fracture zone could be evaluated with both modalities; however, artifacts from metal implants were less noticeable on CRO images compared with CT images (Fig 3). In both patients, the orthopedic fixation devices had been placed correctly.

All CT and CRO studies enabled appropriate diagnosis of the fracture or the postoperative result of fusion. Compared with CT images, transverse CRO images were associated with more artifacts at the transitional areas of thick compact bone, but these artifacts did not influence diagnostic accuracy. Spatial resolution (ie, visualization of the fracture line and small fragments) was better with CRO reconstruction images compared with CT images, and anatomic details could be displayed more precisely. Compared with CT images, the contrast resolution (ie, visualization of the outlines of the bones, differentiation of cortical and spongiosal bone, and differentiation of various soft tissues) was inferior on CRO images. Both observers judged CRO and CT images to have equal quality in two patients; however, CRO images were found to have greater quality with respect to fracture determination in all other patients.

Discussion

CRO provides high-resolution multiplanar and 3D images of complex fractures. Owing to isotropic voxel sizes and superior spatial resolution, anatomic details may be shown more precisely than with thin-section single–detector row spiral CT. For optimized image quality, protocols should be used that have large rotation angles, acquisition of an increased number of projection radiographs per rotation, and high amperage. The spatial resolution on CRO images, which is dependent on the size of the field of view and the reconstruction matrix, is generally superior to that on thin-section single-array CT scans.

The application of digital rotational radiography to anatomic structures other than cerebral arteries has not been reported previously, to our knowledge. However, configuration of the C-arm system, digital radiography software, and postprocessing software should be reevaluated for different applications because the focus on cranial vessel imaging creates several disadvantages for other applications. First, projection images are obtained during forward and backward movement of the C-arm. Dual image assessment is required for rotational digital subtraction angiography (since one data set serves as a mask), but a single rotation would be sufficient for CRO. The additional rotation unnecessarily increases the radiation exposure to the patient. Second, with the current version of the workstation, the reconstruction time was as long as 12 minutes for 512×512-matrix images. This limits applications in which the reformatted and reconstructed images have to be readily available (eg, post- or intraoperative checks).

As would be expected, the contrast resolution on CRO images was less than that on CT scans, but the spatial resolution was superior. CRO images allowed distinction of osseous structures and soft tissue, but various types of soft tissue (eg, fat, muscle) could not be differentiated. The use of improved reconstruction kernels, as are used with CT, and imaging programs with more projection images and increased rotation angle may improve the soft-tissue discrimination.

Our initial results indicate that artifacts due to metal implants influence CRO images less than CT images. However, this should be evaluated prospectively in controlled large-scale studies with different types of orthopedic fixation devices.

We did not measure radiation exposure in our study. Measurements by the manufacturer of the C-arm system showed less radiation exposure for CRO studies than for spiral CT studies (manufacturer's unpublished data). The absorbed dose to air, or CT dose index, on the axis of a cylindric phantom (PMMA; Siemens Medical Solutions) (diameter, 16 cm; length, 14 cm) was 9.7 mGy for the high-dose program at 12 seconds with use of the 40-cm x-ray image intensifier. This is at least half the dose for a standard spiral CT study (absorbed dose, 20–50 mGy, depending on imaging parameters) (manufacturer's unpublished data). However, detailed measurements will have to be performed in the future. Furthermore, the mask rotation is not necessary for CRO. Therefore, a dedicated examination program for CRO should be able to halve the current dose.

For the majority of diagnostic investigations, the spatial resolution provided with spiral CT scanners is sufficient. The higher spatial resolution provided with CRO may help in special cases, such as triplanar fractures of the distal tibia or complex vertebral fractures. With the development of multi–detector row CT, however, similar spatial resolution may be achieved with improved soft-tissue discrimination, which would allow the assessment of associated soft-tissue injuries (16). Therefore, diagnostic investigations, especially in patients suspected of having injuries to other organs (eg, abdominal trauma), will remain the domain of CT. The great advantage of CRO is the capability of cross-sectional imaging in a routine projection imaging system. Therefore, the method would be ideal for guidance of interventional or orthopedic fixation procedures since the results may be checked instantly, and potentially corrected, before the patient leaves the operating room.

If CRO could be implemented within smaller and less expensive portable C-arm systems, such devices could be helpful tools for skeletal interventional radiologists and orthopedic surgeons.

References

1. Kode L, Lieberman JM, Motta AO, Wilber JH, Vasen A, Yagan R. Evaluation of tibial plateau fractures: efficacy of MR imaging compared with CT. AJR Am J Roentgenol 1994; 163:141–147.
2. Liow RY, Birdsall PD, Mucci B, Greiss ME. Spiral computed tomography with two- and three-dimensional reconstruction in the management of tibial plateau fractures. Orthopedics 1999; 22:929–932.
3. Wicky S, Blaser PF, Blanc CH, Leyvraz PF, Schnyder P, Meuli RA. Comparison between standard radiography and spiral CT with 3D reconstruction in the evaluation, classification and management of tibial plateau fractures. Eur Radiol 2000; 10:1227–1232.
4. Fahrig R, Fox AJ, Lownie S, Holdsworth DW. Use of a C-arm system to generate true three-dimensional computed rotational angiograms: preliminary in vitro and in vivo results. AJNR Am J Neuroradiol 1997; 18:1507–1514.
5. Schueler BA, Sen A, Hsiung HH, Latchaw RE, Hu X. Three-dimensional vascular reconstruction with a clinical x-ray angiography system. Acad Radiol 1997; 4:693–699.
6. Grass M, Koppe R, Klotz E, et al. Three-dimensional reconstruction of high contrast objects using C-arm image intensifier projection data. Comput Med Imaging Graph 1999; 23:311–321.
7. Anxionnat R, Bracard S, Macho J, et al. 3D angiography: clinical interest—first applications in interventional neuroradiology. J Neuroradiol 1998; 25:251–262.
8. Missler U, Hundt C, Wiesmann M, Mayer T, Bruckmann H. Three-dimensional reconstructed rotational digital subtraction angiography in planning treatment of intracranial aneurysms. Eur Radiol 2000; 10: 564–568.
9. Liu RR, Rudin S, Bednarek DR. Super-global distortion correction for a rotational C-arm x-ray image intensifier. Med Phys 1999; 26:1802–1810.
10. Fahrig R, Holdsworth DW. Three-dimensional computed tomographic reconstruction using a C-arm mounted XRII: image-based correction of gantry motion nonidealities. Med Phys 2000; 27: 30–38.
11. Wiesent K, Barth K, Navab N, et al. Enhanced 3-D-reconstruction algorithm for C-arm systems suitable for interventional procedures. IEEE Trans Med Imaging 2000; 19:391–403.
12. Fahrig R, Holdsworth DW, Lownie S, Fox AJ. Computed rotational angiography: system performance assessment using in-vitro and in-vivo models. Proc SPIE Med Imaging 1998; 3336:305–315.
13. Mueller ME, Allgoewer M, Schneider R. Manual of internal fixation. 3rd ed. Berlin, Germany: Springer-Verlag, 1991.
14. Magerl F, Aebi M, Gertzbein SD, Harms J, Nazarian S. A comprehensive classification of thoracic and lumbar injuries. Eur Spine J 1994; 3:184–201.
15. Anderson LD, D'Alonzo RT. Fractures of the odontoid process of the axis. J Bone Joint Surg Am 1974; 56:1663–1674.
16. Rydberg J, Buckwalter KA, Caldemeyer KS, et al. Multisection CT: scanning techniques and clinical applications. RadioGraphics 2000; 20:1787–1806.